PHYSICAL REVIEW B **80**, 054513 (2009)

Nanomechanics of an individual vortex in an anisotropic type-II superconductor

E. H. Brandt,[1] G. P. Mikitik,[1,2] and E. Zeldov[3]
[1]*Max-Planck-Institut für Metallforschung, D-70506 Stuttgart, Germany*
[2]*B. Verkin Institute for Low Temperature Physics & Engineering, Ukrainian Academy of Sciences, Kharkov 61103, Ukraine*
[3]*Department of Condensed Matter Physics, Weizmann Institute of Science, Rehovot 76100, Israel*
(Received 18 June 2009; published 18 August 2009)

As shown in recent experiments [Auslaender *et al.*, Nat. Phys. **5**, 35 (2009)] magnetic force microscopy permits one not only to image but also to manipulate an individual vortex in type-II superconductors, and this manipulation provides a new powerful tool to study vortex dynamics and pinning. We derive equations that describe the deformation of an individual vortex in an anisotropic biaxial type-II superconductor under the action of the microscope's magnetic tip. These equations take into account the driving force generated by the tip, the elastic force caused by the vortex deformation, and the pinning force exerted by point defects. Using these equations, we reproduce the main features of the experimental data obtained by Auslaender *et al.*

DOI: 10.1103/PhysRevB.80.054513 PACS number(s): 74.25.Qt, 74.25.Sv

I. INTRODUCTION

In a recent paper[1] magnetic force microscopy (MFM) was employed to image and manipulate individual vortices in a single-crystal $YBa_2Cu_3O_{6.991}$, directly measuring the interaction of a moving vortex with the local disorder potential. Several unexpected results were obtained in that paper. In particular, the authors of Ref. 1 found a dramatic enhancement of the response of a vortex to pulling when they wiggled it transversely. In addition, they discovered enhanced vortex pinning anisotropy in this crystal. These results demonstrate the power of MFM to probe microscopic defects that cause pinning and show that the described manipulations of an individual vortex provide a new powerful tool for studying the vortex dynamics and vortex pinning in type-II superconductors.

In this paper we derive equations that govern the vortex dynamics under such MFM manipulations, and by solving these equations numerically, we provide some insight into the results of Ref. 1.

II. EQUATIONS FOR A MOVING VORTEX

Consider a platelet-shaped biaxial anisotropic superconductor, with its crystalline c axis being perpendicular to the plane of the platelet (and the a and b axes in this plane). Let there be a vortex directed along the c axis in the sample. We denote this axis as the z axis, and choose the x and y axes along the a and b axes of the crystal. MFM employs a sharp magnetic tip placed near the surface of the platelet. The tip magnetization exerts an attractive force $\mathbf{F}$ on the vortex end. This force can shift the top of the vortex when the tip moves. On the other hand, it is possible to measure $\partial F_z/\partial z$ at the tip, and this permits one to visualize the position of the top end of the vortex.[1,2] Let X, Y be the position of the tip in the x-y plane, while its height above the surface of the platelet be Z. We shall describe the shape of the vortex by the functions $x(z)$ and $y(z)$ with $z \le 0$, the position of the vortex end at the surface is thus $x_0 \equiv x(0)$, $y_0 \equiv y(0)$. Below we shall use the following dependence of the force $\mathbf{F}$ on height Z and on the two-dimensional (2D) vector $\mathbf{R} \equiv (X-x_0, Y-y_0)$ (Refs. 1 and 3):

$$\mathbf{F} = q\frac{\mathbf{R} + (Z+h_0)\hat{\mathbf{z}}}{(R^2 + (Z+h_0)^2)^{3/2}}, \tag{1}$$

where the constant $h_0 \approx \lambda$ (λ is on the order of the London penetration depth), $q = \tilde{m}\Phi_0/2\pi$, Φ_0 is the flux quantum, $\tilde{m}$ is the magnetic monopole strength of the tip (or the magnetic moment per unit length of a long narrow cylinder used as tip), and $\hat{\mathbf{z}}$ is the unit vector along the z axis. This dependence is obtained if one considers the tip and the end of a straight vortex as magnetic monopoles of strengths $\tilde{m}$ and $2\Phi_0/\mu_0$.[4] The lateral component of $\mathbf{F}$, $\mathbf{F}_{lat}$, gives the driving force acting on the vortex. The maximum of $\mathbf{F}_{lat}$ with respect to variations of R is reached at $R = (Z+h_0)/\sqrt{2}$ and is equal to[5] $F_m \approx 0.385q/(Z+h_0)^2$. In our following numerical calculations we shall use formula (1) even when the vortex is curved, and to describe the lateral component $\mathbf{f}_{ex}^{\parallel}dz$ of the external driving force applied to a vortex segment which has the projection dz on the z axis, we shall employ the model expression

$$\mathbf{f}_{ex}^{\parallel} = q\frac{\mathbf{R}}{(R^2 + (Z+h_0)^2)^{3/2}}\frac{\exp(-|z|/\lambda)}{\lambda}. \tag{2}$$

This expression can be justified if the change in the total lateral force $\mathbf{F}_{lat}$ on the scale λ in the x-y plane is relatively small (i.e., if $R \gg \lambda$). However, in the case when the vortex shift $(x_0^2+y_0^2)^{1/2}$ caused by the tip is essentially larger than λ, this shift is practically independent of the specific form of the z dependence of $\mathbf{f}_{ex}^{\parallel}$ (see below). So, to clarify the physics without additional mathematical complications, below we shall always use the model dependences (1) and (2).

As it was mentioned above, measurement of $\partial F_z/\partial z$ is employed to visualize the vortex. Equation (1) yields the following expression for this derivative:

$$\left|\frac{\partial F_z}{\partial z}\right| = q\frac{|2(Z+h_0)^2 - R^2|}{(R^2 + (Z+h_0)^2)^{5/2}}. \tag{3}$$

This derivative is maximum $|\partial F_z/\partial z|_{\max} = 2q/(Z+h_0)^3$ when the tip is just above the vortex, i.e., when $X = x_0$, and $Y = y_0$. On the other hand, the maximum lateral force occurs when

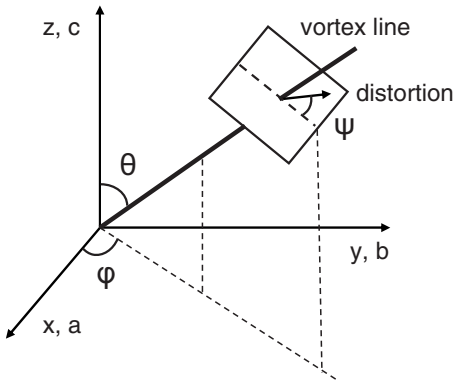

FIG. 1. Definition of the angles θ, φ, and ψ. The angles θ and φ specify the direction of the vortex shown as bold solid line. The angle ψ in the plane perpendicular to the vortex defines the direction of the pinning force; ψ is measured from the line that is the intersection of this plane with the plane containing the vortex and the z axis.

$R=(Z+h_0)/\sqrt{2}$, and hence $|\partial F_z/\partial z|=q(2/3)^{3/2}/(Z+h_0)^3 \approx 0.27|\partial F_z/\partial z|_{\max}$ at this R. In other words, the maximum of the lateral force and the maximum of $|\partial F_z/\partial z|$ occur at different positions of the tip and of the vortex end.

We shall consider the vortex as an elastic string. In the case of a biaxial superconductor the line tension of the vortex, $\varepsilon_l(\theta,\varphi,\psi)$, and the pinning force acting on its unit length, $f_p(\theta,\varphi,\psi)$, were calculated in Ref. 6. The angles θ and φ define the direction of the vortex, i.e., we shall describe this direction by the unit vector

$$(\sin\theta\cos\varphi,\sin\theta\sin\varphi,\cos\theta)=\frac{(x',y',1)}{\sqrt{1+x'^2+y'^2}}, \quad (4)$$

while the angle ψ defines the direction of the pinning force or of the vortex distortion in the plane perpendicular to the vortex, Fig. 1. Here the prime means d/dz. In the subsequent analysis the line tension will be required only for the case $\theta=0$ since the linear elasticity theory is valid up to sufficiently large angles θ if the parameter ε is small.[7] Then, we have[1,6]

$$\varepsilon_l(\varphi,\psi)=\varepsilon_0\varepsilon^2\eta(\varphi+\psi)\equiv\varepsilon_l(\varphi+\psi), \quad (5)$$

where $\varepsilon\equiv\lambda_{ab}/\lambda_c$ is the parameter of the anisotropy; $\varepsilon_0=(\Phi_0/\lambda_{ab})^2\ln(\lambda_{ab}/\xi_{ab})/(4\pi\mu_0)$; $\lambda_{ab}=\sqrt{\lambda_a\lambda_b}$; λ_c, λ_a, and λ_b are the London penetration depths, $\zeta=\lambda_a/\lambda_b$ is the parameter of the anisotropy in the a-b plane, and

$$\eta(\varphi)=\zeta\cos^2\varphi+\zeta^{-1}\sin^2\varphi. \quad (6)$$

Since at $\theta=0$ the plane perpendicular to the vortex coincides with the x-y plane, the combination $\varphi+\psi$ in Eq. (5) is the angle defining the direction of the vortex distortion in this plane relative to the x axis.[8] As to the pinning force, it is described by the expression[6]

$$f_p(\theta,\varphi,\psi)=f_p^c\frac{\xi_{ab}\cos\theta}{\xi(\theta,\varphi,\psi)}, \quad (7)$$

where f_p^c is the pinning force for the vortex along the c axis in the uniaxial superconductor with the same λ_{ab} and $\xi_{ab}=\sqrt{\xi_a\xi_b}$. Here ξ_a and ξ_b are the coherence lengths, and

$$\xi^2(\theta,\varphi,\psi)=\xi_{ab}^2\left[\zeta(\sin\varphi\cos\psi\cos\theta+\cos\varphi\sin\psi)^2+\frac{1}{\zeta}(\cos\varphi\cos\psi\cos\theta-\sin\varphi\sin\psi)^2\right]. \quad (8)$$

In $YBa_2Cu_3O_{6.99}$ one has[9] $\varepsilon\approx 1/7$ (i.e., $\varepsilon^2\ll 1$) and[1,9] $\zeta\approx 1.3$.

Consider a vortex segment limited by the planes z and $z+dz$ and specified by the angles θ and φ. Let us analyze the balance of the driving, the pinning, and the elastic forces applied to this segment. All these forces are perpendicular to it. However, to find the two functions $x(z)$ and $y(z)$ describing the vortex, it is convenient to carry out the analysis in the x-y plane, projecting all the forces onto this plane. The projection of the elastic force acting on this segment, $\mathbf{f}_{el}^{\parallel}dz$, can be described by the simple expression $\mathbf{f}_{el}^{\parallel}dz=(\varepsilon_{lx}x'',\varepsilon_{ly}y'')dz$ even at sufficiently large θ since the linear elasticity theory is valid up to the angles satisfying $\varepsilon^2\tan^2\theta\ll 1$.[7] Here $\varepsilon_{lx}=\varepsilon_l(0)=\varepsilon_0\varepsilon^2\zeta$ and $\varepsilon_{ly}=\varepsilon_l(\pi/2)=\varepsilon_0\varepsilon^2/\zeta$ are the appropriate line tensions at $\theta=0$ [see Eqs. (5) and (6)]. Adding this projection of the elastic force to the external force defined by Eq. (2), one obtains the projection $\mathbf{f}^{\parallel}dz$ of the resultant force $\mathbf{f}dz$ on the x-y plane. Then, the *first* of two equations for $x(z)$ and $y(z)$ is

$$f^{\parallel}(x,y,X,Y)=f_c^{\parallel}, \quad (9)$$

where $f_c^{\parallel}$ is the absolute value of the projection of the so-called critical force[6] on the x-y plane. This critical force is the force at which the vortex starts to move. It is determined by the pinning force, but in the anisotropic superconductor it can differ from the pinning force.[6] Note that we write one Eq. (9) which connects the absolute values of $\mathbf{f}^{\parallel}$ and $\mathbf{f}_c^{\parallel}$ rather than two equations for the x and y components of these forces. This is due to the fact that the direction of the pinning force (and hence of the critical force) is not known in advance and is dictated by the direction of $\mathbf{f}^{\parallel}$.

The critical force $f_c^{\parallel}$ is determined by the following formulas: let the direction of the force $\mathbf{f}$ be specified by the angle ψ in the plane perpendicular to the vortex. This angle can be expressed in terms of the component $f_x^{\parallel}$ and $f_y^{\parallel}$ of the force $\mathbf{f}^{\parallel}$ as follows:

$$\tan\psi=\frac{\cos\theta(f_y^{\parallel}-f_x^{\parallel}\tan\varphi)}{f_x^{\parallel}+f_y^{\parallel}\tan\varphi}. \quad (10)$$

The pinning force f_p in the direction ψ is given by Eqs. (7) and (8), while the critical force f_c in this direction ψ is determined by[6]

$$\tan(\psi-\psi_1)=\frac{f_p'(\psi_1)}{f_p(\psi_1))}, \quad (11)$$

$$f_c(\psi)=\sqrt{[f_p(\psi_1)]^2+[f_p'(\psi_1)]^2}, \quad (12)$$

where the prime means $d/d\psi_1$, and the angle ψ_1 in the plane perpendicular to the vortex defines the direction along which the vortex starts to move when the force acting along ψ exceeds f_c. The fact that ψ_1 in general differs from ψ is due

to the anisotropy of the pinning. On determining ψ_1 from Eq. (11), one then finds $f_c(\psi)$ from formula (12). The explicit form of Eqs. (11) and (12) for the case of the pinning force described by formulas (7) and (8) is presented in Appendix A. Finally, when the critical force $f_c(\psi)$ is found, its projection $f_c^{\parallel}$ on the x-y plane is determined by the formula

$$f_c^{\parallel} = f_c(\psi)\frac{(\cos^2\theta\cos^2\psi+\sin^2\psi)^{1/2}}{\cos\theta}, \tag{13}$$

that follows from geometrical considerations.

Equation (9) is a differential equation since it contains the derivatives $x''(z)$ and $y''(z)$ originating from the elastic force. As in Ref. 1, we shall consider only sufficiently thick superconducting crystals in which the vortex as a whole does not shift, and only its upper part $(0 \geq z \geq z_0)$ adjoining the x-y surface moves, while the lower part $(z < z_0)$ is pinned. The boundary point z_0 of this upper part is determined by

$$x(z_0) = y(z_0) = 0. \tag{14}$$

Then, the boundary conditions to Eq. (9) are

$$x'(z_0) = y'(z_0) = 0, \tag{15}$$

$$x'(0) = y'(0) = 0. \tag{16}$$

If these conditions were not fulfilled, the derivatives x' and y' would be discontinuous at the points $z=z_0$ and $z=0$, and the elastic force $(\varepsilon_{lx}x'', \varepsilon_{ly}y'')$ would be singular there.[10] In the most interesting case when $x_0^2+y_0^2 \gg \lambda^2$ (and hence $|z_0| \gg \lambda$), one can put $\lambda \to 0$. In this limiting case the driving-force $\mathbf{F}$ is applied to the vortex only at its surface point (x_0, y_0). Then, in Eq. (9) the force $\mathbf{f}_{ex}^{\parallel}$ can be omitted, $\mathbf{f}^{\parallel}$ coincides with $\mathbf{f}_{el}^{\parallel}$, and the driving-force $\mathbf{F}$ only modifies the boundary condition (16). Now the integration of the forces over the thickness of the surface layer gives

$$x'(0) = \frac{F_x}{\varepsilon_{lx}}, \quad y'(0) = \frac{F_y}{\varepsilon_{ly}}. \tag{17}$$

This result shows that at small λ the vortex dynamics is practically independent of the distribution of the driving-force $\mathbf{F}$ over the surface layer of thickness λ.

Equation (9) alone is not sufficient to find the two functions $x(z)$ and $y(z)$. We now derive a *second* equation for these functions. When the position of the tip changes, the vortex begins to move in the direction ψ_1 in the plane perpendicular to the vortex. This movement of the vortex in the perpendicular plane corresponds to its shift at an angle $\tilde{\psi}_1$ (measured from the x axis) in the x-y plane. A geometrical consideration shows that this angle $\tilde{\psi}_1$ is determined by

$$\tan\tilde{\psi}_1 = \frac{\tan\varphi+\cos\theta\tan\psi_1}{1-\cos\theta\tan\varphi\tan\psi_1}. \tag{18}$$

Thus, changes in the functions $x(z)$ and $y(z)$ in time are connected by the relation

$$\frac{dy}{dt} = \tan\tilde{\psi}_1\frac{dx}{dt}. \tag{19}$$

This is a second equation for the functions $x(z)$ and $y(z)$. Since the time t can be expressed in terms of the known functions $X(t)$, $Y(t)$ that describe the shift of the tip, Eq. (19) and its solution (i.e., the shape of the vortex at some moment t_0) depend on the *trajectory* $Y(X)$ of the tip in the x-y plane at previous times $(t < t_0)$ rather than on a specific form of the temporal dependences $X(t)$ and $Y(t)$. This situation is reminiscent of the case that occurs in the theory of the critical states of type-II superconductors when the external magnetic field $\mathbf{H}_a$ applied to a superconducting sample changes in a complex way.[11,12] In this case the critical states are different for different histories $\mathbf{H}_a(t)$ with the same final value of $\mathbf{H}_a$.

Equations (1)–(19) describe the vortex dynamics in thick superconducting crystals when the tip moves in its x-y plane. We solve these equations in the next section.

III. RESULTS

The equations of the previous section show that if the driving-force density $f_{ex}^{\parallel}$ at the surface of the superconductor, $z=0$, is lower than a certain threshold $f_c^{\parallel}(\alpha)$ where α is the angle of $\mathbf{f}_{ex}^{\parallel}$ relative to the x axis, the vortex remains pinned, i.e., $x(z)=y(z)=0$. In particular, if the driving force acts along the x or y direction, we obtain the following thresholds: $f_p^c\sqrt{\zeta}$ and $f_p^c/\sqrt{\zeta}$, respectively, which coincide with the appropriate pinning forces. Here we have used the formulas of Appendix A and the fact that $\delta = 1/\zeta^2 > 1/2$ at the experimental value[1,9] of $\zeta = 1.3$. Equivalently, these threshold conditions can be rewritten in terms of the total forces, $F_x \leq F_{px} \equiv f_p^c\lambda\sqrt{\zeta}$ and $F_y \leq F_{py} \equiv f_p^c\lambda/\sqrt{\zeta}$. If the driving force exceeds the threshold values only a little, i.e., if $F_x - F_{px} \ll F_x$, or $F_y - F_{py} \ll F_y$, we find from the equations that x_0 or y_0 begins to deviate gradually from zero,

$$x_0 \approx \frac{2\lambda(F_x-F_{px})^3}{\varepsilon_{lx}F_x^2}, \quad y_0 \approx \frac{2\lambda(F_y-F_{py})^3}{\varepsilon_{ly}F_y^2}. \tag{20}$$

With further increase in the driving force, at $F_x \gg F_{px}$ or $F_y \gg F_{py}$ but at the same time under the conditions $F_x \ll \varepsilon_{lx} = \zeta\varepsilon^2\varepsilon_0$ or $F_y \ll \varepsilon_{ly} = \varepsilon^2\varepsilon_0/\zeta$, we arrive at

$$x_0 \approx \frac{F_x(F_x-2F_{px})}{2\zeta^{3/2}f_p^c\varepsilon^2\varepsilon_0}, \quad y_0 \approx \frac{\zeta^{3/2}F_y(F_y-2F_{py})}{2f_p^c\varepsilon^2\varepsilon_0}. \tag{21}$$

The additional conditions $F_x \ll \varepsilon_{lx}$, $F_y \ll \varepsilon_{ly}$ mean that the characteristic tilt angle θ of the vortex is small [see Eqs. (17) in which $x'(0)$, $y'(0)$ are just equal to $\tan\theta$]. This smallness of θ was assumed in Ref. 1 in analyzing the vortex dynamics, and formulas (21) coincide with those obtained in that paper. However, F_{px}/ε_{lx}, F_{py}/ε_{ly} are not necessarily small in an experiment. In this case formulas (21), strictly speaking, have no region of applicability. Moreover, boundary conditions (17) show that the characteristic tilt angle θ is not small at typical experimental values of $F_{x,y} \sim 5-20$ pN even when $\varepsilon_{lxy} \sim 10$ pN. So we do not assume in this paper that $\tan\theta \ll 1$. The equations of the previous section have been derived only under a weaker condition $\varepsilon^2\tan^2\theta \ll 1$. But when θ

~ 1, the critical force f_c differs from f_p even for symmetry directions.[6] For example, when the tip moves along x and thus the vortex also bends along this direction, formula (A5) of Appendix A gives

$$f_c^{\parallel}(\theta) = f_p^c\sqrt{\zeta}, \quad \tan^2\theta \le \frac{2}{\zeta^2} - 1;$$

$$f_c^{\parallel}(\theta) = \frac{2f_p^c}{\zeta^{3/2}}\cos\theta\sqrt{\zeta^2 - \cos^2\theta}, \quad \tan^2\theta \ge \frac{2}{\zeta^2} - 1, \quad (22)$$

while for the tip moving along the y axis, one has

$$f_c^{\parallel}(\theta) = \frac{f_p^c}{\sqrt{\zeta}}, \quad \tan^2\theta \le 2\zeta^2 - 1;$$

$$f_c^{\parallel}(\theta) = 2\zeta^{1/2}f_p^c\cos\theta\sqrt{1 - \zeta^2\cos^2\theta}, \quad \tan^2\theta \ge 2\zeta^2 - 1. \quad (23)$$

In other words, even at moderate θ the critical force begins to depend on this angle, and the formulas for x_0 and y_0 become more complicated than Eqs. (21) in which $f_c^{\parallel}$ was assumed to be constant and to coincide with the appropriate pinning force, $f_c^{\parallel}(\theta) = f_p^c\sqrt{\zeta}$ at $\varphi = 0$ and $f_c^{\parallel}(\theta) = f_p^c/\sqrt{\zeta}$ at $\varphi = \pi/2$. Such a dependence of $f_c^{\parallel}(\theta)$ in general causes that the ratio y_0/x_0 at large driving forces differs from the value $\zeta^3 \approx 2.2$ that follows from formulas (21). This may lead to an imitation of the enhanced pinning anisotropy observed by Auslaender *et al.*,[1] see below.

During its motion the vortex lags behind the moving tip until the maximum lateral force is reached at $r_m = \max(x_0^2 + y_0^2)^{1/2}$. At small driving force the vortex will remain at this r_m, whereas at large driving forces the vortex will, in fact, partially recede after the tip has moved away. Experimentally the final location of the vortex is evaluated on the returning path of the tip by monitoring the tip location $R_m \equiv (X^2 + Y^2)^{1/2}$ at which $\partial F_z/\partial z$ is maximum when the tip is above the vortex (or closest to it). In Fig. 2 we show the maximum shift of the vortex end, r_m, in the forward direction and R_m on the returning path of the tip vs. the driving force when the tip moves either along the x axis or along the y axis. In these cases the vortex shifts along these symmetric directions, too. Figure 2 shows that at low driving forces the experimentally determined R_m accurately reproduces the maximum shift of the vortex r_m whereas at higher forces R_m slightly underestimates the actual r_m.

In the construction of Fig. 2, as well as Figs. 3 and 4, we put $\zeta = 1.3$ and measure forces in units of the line tension $\varepsilon_{lxy} \equiv (\varepsilon_{lx}\varepsilon_{ly})^{1/2} = \varepsilon^2\varepsilon_0$, and lengths in units of λ (hence the force densities f_p, f_c, f_{el}, and $f_{ex}^{\parallel}$ are in units of $\varepsilon_{lxy}/\lambda$). Then, taking into account the model dependence (2) for the driving-force density $f_{ex}^{\parallel}$, one finds that Eqs. (9) and (19) for $x(z)$ and $y(z)$, as well as the boundary condition (17), become independent of the absolute values of ε_0, ε, and λ. They depend only on the dimensionless forces $F_{x,y}/\varepsilon^2\varepsilon_0$ and the dimensionless parameter $P \equiv f_p^c\lambda/\varepsilon^2\varepsilon_0$. Thus, in a certain sense Fig. 2 is universal. But in this scaling procedure one has to bear in mind that if one changes the parameter λ keeping a fixed value of $F_{x,y}/\varepsilon^2\varepsilon_0$, this leads to a change in the tip position X, Y which is not scaled with λ [see Eq. (1)]. However, if one is interested only in the tip position when it is just above the vortex, the scaling still holds in this case. On the other hand, when the relative positions of the tip and of the vortex are essential (e.g., in the construction of Figs. 5–13), we use the following set of input parameters:

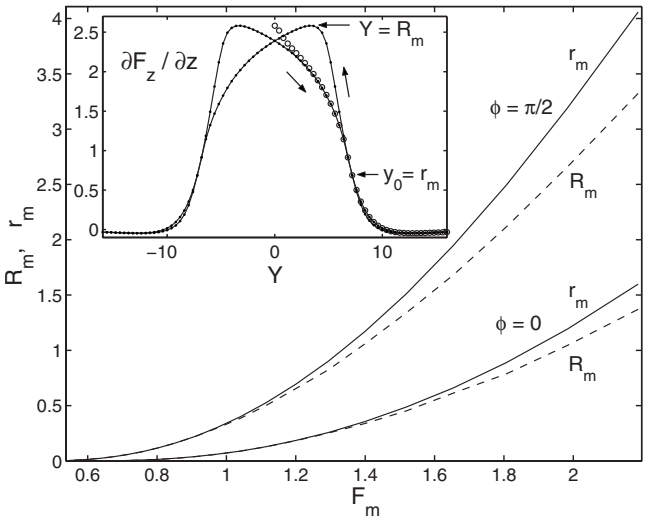

FIG. 2. Dependence of the maximum shift of the vortex end, $r_m \equiv \max(x_0^2 + y_0^2)^{1/2}$, on the driving-force F_{mx} or F_{my} when the tip moves along the x axis ($\varphi = 0$) or the y axis ($\varphi = \pi/2$). The forces are measured in units of the line tension $\varepsilon_{lxy} \equiv \varepsilon^2\varepsilon_0$, the lengths in units of λ, $\zeta = 1.3$, and $P \equiv f_p^c\lambda/\varepsilon_{lxy} = 0.5$. The dashed lines show the appropriate X and Y positions of the tip, $R_m \equiv (X^2 + Y^2)^{1/2}$, at which the derivative $\partial F_z/\partial z$ reaches its maximum on the returning path. As an example, the Y dependence of this derivative at $\phi = \pi/2$ and $F_{my}/\varepsilon_{lxy} \approx 2.2$ is presented in the inset. The circles in the inset mark the virgin curve, and the arrows indicate the direction of the tip motion.

$$\lambda = 0.2\ \mu\text{m}, \quad \varepsilon_{lxy} \equiv (\varepsilon_{lx}\varepsilon_{ly})^{1/2} = 9\ \text{pN},$$

$$P = \frac{f_p^c\lambda}{\varepsilon_{lxy}} = 0.5, \quad \frac{q}{\varepsilon_{lxy}} = 1.1\ \mu\text{m}^2, \quad Z + h_0 = 0.44\ \mu\text{m}. \quad (24)$$

The data of Fig. 2 are similar to the data of Fig. 3b in Ref. 1. Moreover, a semiquantitative agreement of these data can be obtained if one takes λ on the order of several tenths of a micron and $\varepsilon_{lxy} \sim 10$ pN. However, this value of the line tension ε_{lxy} is 10–20 times larger than the theoretical estimate of this quantity, $\varepsilon_{lxy} = \varepsilon^2(\Phi_0/\lambda_{ab})^2\ln(\lambda_{ab}/\xi_{ab})/(4\pi\mu_0)$, at $\varepsilon = 1/7$, $\lambda_{ab} = 0.2$ μm, and $\ln(\lambda_{ab}/\xi_{ab}) = 4$. Thus, apart from an enhanced anisotropy of pinning discovered by Auslaender *et al.*,[1] their experimental data in fact means that either the vortex has an enhanced line tension, or the model dependences (1) and (2) for the driving force are oversimplified under the conditions of the experiment and lead to an essential overestimation of this force.

In Fig. 3 that is similar to Fig. 4c of Ref. 1, we show the dependence of the maximum shift of the vortex end, r_m, on the angle φ at which the tip moves along a straight line in the x-y plane at a certain height Z above the surface of the su-

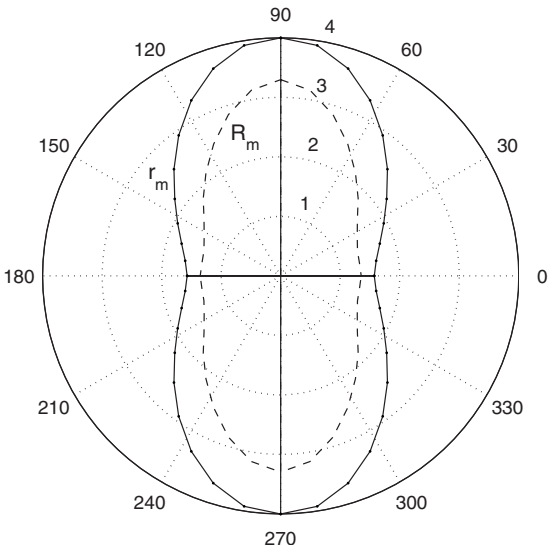

FIG. 3. Polar plot of the maximum shift r_m of the vortex-end $r=(x_0^2+y_0^2)^{1/2}$ versus the angle φ of the tip motion (solid line). The tip moves along a straight line in the X-Y plane with a sufficiently large amplitude and at the height Z that leads to $F_m/\varepsilon_{lxy}\approx 2.2$. The dashed line shows the shift $R_m=(X^2+Y^2)^{1/2}$ of the tip when the derivative $\partial F_z/\partial z$ reaches its maximum. Length unit is λ, $P=0.5$, $\zeta=1.3$.

perconductor. This height determines the maximum driving-force F_m applied to the vortex, and in Fig. 3 this height is chosen so that $F_m/\varepsilon_{lxy}\approx 2.2$. For comparison, we again show the positions of the tip, $R_m\equiv(X^2+Y^2)^{1/2}$, at which the derivative $\partial F_z/\partial z$ reaches its maximum. The anisotropy of the vortex shift, $r_m(\varphi=\pi/2)/r_m(\varphi=0)\approx 2.5$, seen in the figure approximately coincides with the ratio $R_m(\varphi=\pi/2)/R_m(\varphi=0)$, and at $\zeta=1.3$ this anisotropy is lower than the appropriate experimental value ~3.5.[1] This experimental value can be fitted if one takes $\zeta=1.43$. Thus, although this $\zeta=1.43$ obtained with taking into account the θ dependence of $f_c^{\|}$ is less than $\zeta=1.6$ derived in the simplified analysis,[1] our approach still cannot completely describe the enhanced anisotropy of pinning within the framework of collective pinning theory by point defects. Auslaender *et al.*[1] suggested that this enhanced anisotropy is due to a clustering of the point defects.

Interestingly, when the tip moves along a straight line different from the x and y axes, the trajectory of the vortex end performs a "hysteresis loop" with its axis deviating from the direction of tip motion, Fig. 4. Also depicted in Fig. 4 is the six times enlarged path near the first and the second turns, showing that the vortex end reaches maximum elongation, then it recedes when the tip moves away, and when the tip returns, the vortex end approaches the tip and reaches maximum elongation a second time. These results clearly demonstrate that the vortex in general moves in a direction different from the direction of the tip motion, and that the vortex position depends on the trajectory of the tip at previous times.

In Ref. 1 the derivative $(\partial F_z/\partial z)$ was measured when the tip oscillates with a large amplitude along some line and at the same time it is slowly shifted in the perpendicular direction. In this case an enhanced shift of the vortex along the slow scan direction was discovered (see Figs. 1 and 2 in Ref. 1). We have investigated this situation theoretically. In Fig. 5 the zigzag path $x_0(t)$, $y_0(t)$ of the vortex end is presented

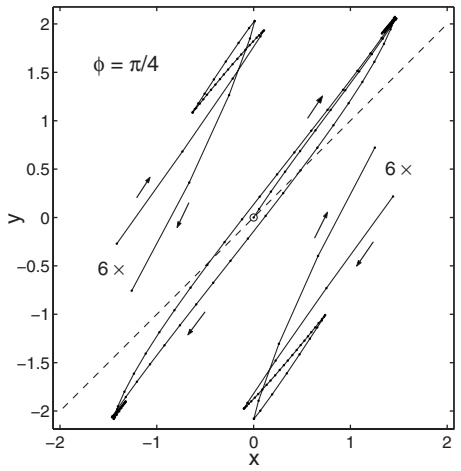

FIG. 4. Path of the vortex-end $x(t)$, $y(t)$ when the tip oscillates along the diagonal $X(t)=Y(t)$ (dashed line) with a large amplitude; same data as in Fig. 3. Both the tip and the vortex start at $x=y=0$. Length unit is λ, $P=0.5$. The vortex path cycles a narrow hysteresis loop as indicated by the arrows. Due to the in-plane anisotropy $\zeta=1.3$, this loop is tilted away from the tip path ($\varphi=\pi/4$) toward the y axis. Also depicted is the six times enlarged and shifted path near the first and the second turns. The dots on the curves are at equidistant times.

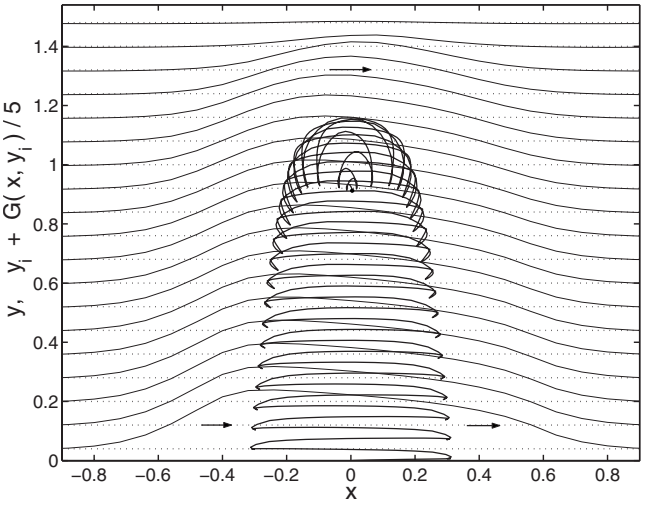

FIG. 5. The zigzag path $x_0(t)$, $y_0(t)$ of the vortex end (bold lines in the center) when the tip oscillates with large amplitude $a=1.6$ μm along x and at the same time moves slowly up along y, with $\dot{Y}/|\dot{X}|=1/80$. Tip and vortex start at $x=y=0$. Length unit is μm, $\zeta=1.3$, the other parameters are listed in Eqs. (24). The aspect ratio of this path is $\max(y_0)/\max(x_0)\approx 3.7$. The almost horizontal dotted lines at equidistant $y=y_i$ show the tip path when it moves from the left to the right (see arrows) and serve as zero lines for the force derivative $g(x,y_i)=\partial F_z/\partial z$ plotted versus x as $y_i+0.2\cdot G(x,y_i)$ (solid lines) with $G=g/\max(|g|)$. Note that these curves are asymmetric due to the unidirectional tip motion shown here. The return path yields similar curves, obtained from the depicted curves by the reflection $x\to -x$.

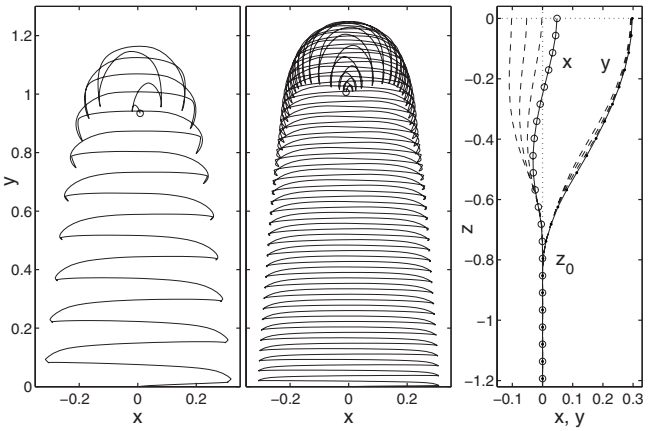

FIG. 6. The zigzag path $x_0(t)$, $y_0(t)$ of the vortex end as in Fig. 5 but at $\dot{Y}/|\dot{X}|=1/40$ (left plot, $\max(y_0)/\max(x_0)\approx 3.6$) and at $\dot{Y}/|\dot{X}|=1/160$ (middle plot, $\max(y_0)/\max(x_0)=4.1$). The right plot shows the vortex shape expressed as $x(z)$ (solid line with circles) and $y(z)$ (solid line with dots) at the moment when $x_0=0.05$, $y_0=0.3$ in the left plot. The dashed lines show these functions at three previous time steps.

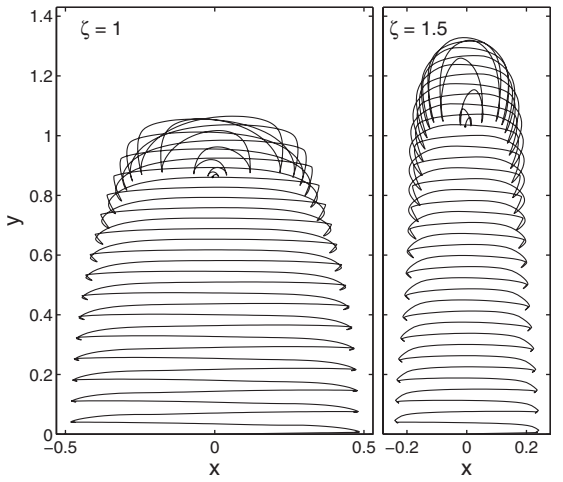

FIG. 7. The zigzag path $x_0(t)$, $y_0(t)$ of the vortex end as in Fig. 5 but for $\zeta=1$ (left plot) and $\zeta=1.5$ (right plot). The aspect ratio $\max(y_0)/\max(x_0)$ is approximately 2.2 for $\zeta=1$ and 5.5 for $\zeta=1.5$.

when the tip oscillates with a large amplitude along x and at the same time moves slowly up along y. We also show the X profiles of $(\partial F_z/\partial z)$ at various fixed values of Y. Note that these profiles are asymmetric and are different for tip motion from left to right and from right to left. The data of Fig. 5 qualitatively reproduces the experimental data.[1] Interestingly, this figure also clearly shows how the elastic force drags the vortex back toward the origin when the tip goes far away from the vortex.

In Fig. 6 we compare the vortex paths for various ratios of the scan rates along x and y. It is seen that the results are different for different rates although we do not take into account the effect of vortex creep here. This difference in the vortex paths is due to the above-mentioned dependence of the vortex position on the trajectory of the tip at previous times. In this figure we also present the vortex-shape functions $x(z)$ and $y(z)$ at some moment of time. These functions show that during the zigzag motion the vortex is bent and twisted into a complicated shape. The lower part $z\leq z_0$ of the vortex is rigidly pinned (has exactly $x=y=0$) and at the surface $z=0$ the vortex ends perpendicularly. We find that for the tip motion of Fig. 6, at $z>z_0$ the component $y(z)$ increases with z monotonically, while $x(z)$ after several scan periods exhibits strongly damped oscillations.

In Fig. 7 we analyze the dependence of the zigzag vortex motion on the anisotropy parameter ζ. It is clear from the figure that the shift of the vortex end in the slow scan direction and the aspect ratio $\max(y_0)/\max(x_0)$ increase[13] with increasing ζ. But importantly, even in the case of isotropic pinning in the x-y plane, i.e., at $\zeta=1$, this aspect ratio remains considerably larger than unity. From a qualitative point of view, this enhanced tilt of the vortex along y is caused by the fact that during the zigzag motion the vortex predominately moves in the x direction, the pinning force is also directed mainly along x, and hence this force opposes only the vortex tilt in the x direction. These considerations are supported by the data of Fig. 8 in which for the case of a small λ we show $x(z)$, the maximum displacement of the vortex when the tip moves only along the x axis (i.e., during the first oscillation of the tip in the left plot of Fig. 7), and $y(x)$ at the moment when y_0 reaches its maximum value after many oscillations of the tip. Since at small λ the driving force concentrates near the surface of the superconductor, in the bulk of the sample the elastic force associated with the curvature of the vortex has to be balanced mainly by the pinning force. Then, the *long straight segment* of the line

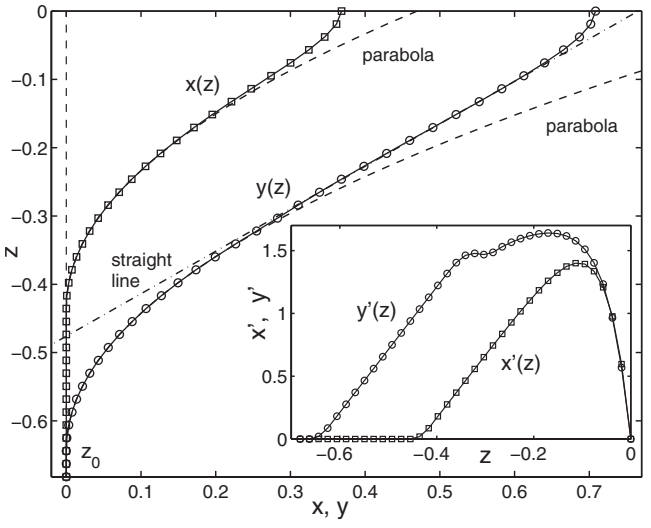

FIG. 8. The vortex shape during oscillations of the magnetic tip above a superconductor that is isotropic in the a-b plane ($\zeta=1$). Similar case as the left plot of Fig. 7, but to clarify the situation, we take $\lambda_{ab}=0.05$ μm and $P=0.25$ here. Shown are the maximum vortex displacement $x(z)$ at the first excursion of the tip (i.e., at $Y=0$) and the maximum displacement $y(z)$ at the moment when $x_0=0$ while y_0 reaches its maximum value after many tip oscillations. The dash-dotted straight line reveals that the curve $y(z)$ has a long zero-curvature segment, see also $x'(z)$ and $y'(z)$ shown in the inset (the small hump seen in the flat part of $y'(z)$ oscillates in time). At small x and y both $x(z)$ and $y(z)$ are parabolas with curvature f_p^c/ε_{lxy} (dashed lines).

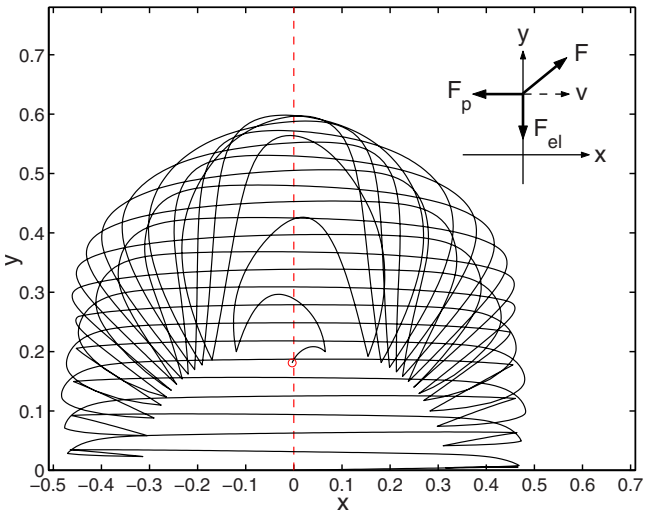

FIG. 9. (Color online) Path of the vortex end and force balance for a simplified 2D model, see text. The tip moves as in Fig. 7, the left plot. Here $Z+h_0=0.44$ μm, $q=9.9$ μm$^2\cdot$pN (which gives $F_m \approx 20$ pN); $F_p=F_m/4$; $\zeta=1$; $k_x=k=32$ pN/μm; x and y are measured in μm. The aspect ratio $r\equiv \max(y_0)/\max(y_0)\approx 1.24$. The force balance is shown for the point $(x_0,y_0)=(0,\max(y_0))$.

$y(z)$ shown in Fig. 8 means that the y component of the pinning force is practically absent in this segment.

Some insight into the origin of the vortex-motion anisotropy seen in Fig. 7 can be also obtained from a simplified two-dimensional (2D) model. In this model we disregard the dynamics of the entire vortex and consider only the vortex end as a point (x_0,y_0) elastically connected to the origin of the x-y plane, $\mathbf{F}_{el}=-(k_x x_0,k_y y_0)$, where k_x and $k_y=k_x/\zeta^2$ are some spring constants modeling the elasticity of the vortex. In this simplified approach the problem of the vortex motion becomes two-dimensional, and instead of the force densities we deal with the elastic force $\mathbf{F}_{el}$, the total pinning force $\mathbf{F}_p$, and the driving-force $\mathbf{F}_{lat}=(F_x,F_y)$ determined by Eq. (1). The balance of these three forces and the vortex-end motion can be still described by the equations of Sec. II if one puts $\theta=\varphi=0$ and replaces the force densities by the total forces in the equations. Interestingly, in this simplified 2D approach one can qualitatively reproduce the main results which have been obtained above accounting for the real three-dimensional (3D) shape of the vortex. In particular, in Fig. 9 we show the zigzag path of the vortex end in the case $\zeta=1$ (isotropic elasticity and pinning in the x-y plane). In the construction of this figure we use the same parameters for the tip as in Fig. 7 (i.e., we have $F_m \approx 20$ pN). Besides this, we take $F_p=F_m/4\approx 5$ pN. This relation also corresponds to the case of Fig. 7 if one implies that F_p for the 2D model is equal to $f_p^c\lambda$. Such choice of F_p is dictated by a comparison of the conditions $F_m \geq F_p$ and $F_m \geq f_p^c\lambda$ for a vortex to start to move in the simplified 2D model and in the 3D theory. The spring constant in Fig. 9 is chosen such that $\max(x_0)$ is the same as in the left plot of Fig. 7. The vortex trajectory presented in Fig. 9 reveals the anisotropy of the vortex motion in the y and x directions with the aspect ratio $r\equiv \max(y_0)/\max(x_0) \approx 1.24$. This anisotropy can be understood from the following simple considerations: The maximum displacement of the vortex end along x is found from

$$\max(x_0)=\frac{F_m-F_p}{k}, \tag{25}$$

where F_m is the maximum value of the driving force and $k \equiv k_x$. The y_0 reaches its maximum when $x_0\approx 0$, the vortex-end velocity v is practically parallel to x, and thus the pinning force is along this axis, too, (Fig. 9). The driving force at this moment is maximum, $F=F_m$, and is directed at an angle α with respect to the x axis, while the elastic force acts toward the origin. Then, the force balance for the x and y components gives

$$F_m \cos\alpha = F_p, \quad F_m \sin\alpha = k \max(y_0), \tag{26}$$

and hence $\max(y_0)=F_m \sin\alpha/k=\sqrt{F_m^2-F_p^2}/k$. The aspect ratio is therefore

$$r=\frac{\max(y_0)}{\max(x_0)}=\sqrt{\frac{F_m+F_p}{F_m-F_p}}>1, \tag{27}$$

and it is independent of k. If $F_m \to F_p$ the ratio r diverges, but in this case the vortex displacements are small and become less than the vortex radius which is on the order of λ_{ab} for MFM. For F_m and F_p of Fig. 9 formula (27) yields the aspect ratio $r=\sqrt{5/3}\approx 1.29$, which is indeed close to that found in this figure.

In Fig. 10 we analyze one more effect that was observed experimentally [see Figs. 4c and 4d in Ref. 1]. At the initial-time $t=0$, the straight vortex is at $x=y=0$. The tip oscillates along x with a large amplitude and slowly approaches the vortex from large positive y. At a certain time the end of the vortex abruptly jumps to the tip and then begins to oscillate with a large amplitude. This effect of a sharp onset of the signal is qualitatively reproduced by our Fig. 10. A close look to Fig. 10 shows that the large jump of the vortex end is composed of several jumps of width increasing nearly exponentially in time. These multiple jumps are even better seen in Fig. 11 that shows how the vortex end moves when the tip oscillates along y and slowly moves along x starting far away from the waiting vortex. As compared to the corresponding Figs. 5, 6, and 10 which are described by the same parameters and have a vortex-path aspect ratio $\max(y_0)/\max(x_0) \approx 4$, in Fig. 11 the aspect ratio $\max(x_0)/\max(y_0)\approx 1.3$ is smaller than even that for the isotropic case (≈ 2.2) since the pinning anisotropy now impedes[13] the vortex motion in the x direction.

In Fig. 12 we reproduce one more experiment described in Ref. 1 (in the supplementary material). In this experiment the tip oscillates along a straight line at $t>0$ and does not shift in the perpendicular direction. The vortex that waits at some distance from the line of the tip oscillations at $t\leq 0$, at $t>0$ begins to move toward the tip. Figure 12 shows this attraction process for the isotropic case $\zeta=1$ and for the tip-oscillations line parallel to the x axis. The initial shift $y_0(0)$ of the vortex end along y occurs at $t\leq 0$ when the tip approaches its starting point from large positive Y. This shift occurs if the driving force at $t=0$ exceeds the appropriate pinning force $F_p=f_p^c\lambda$. If the initial distance of the vortex from the tip-oscillations line is so large that the driving force

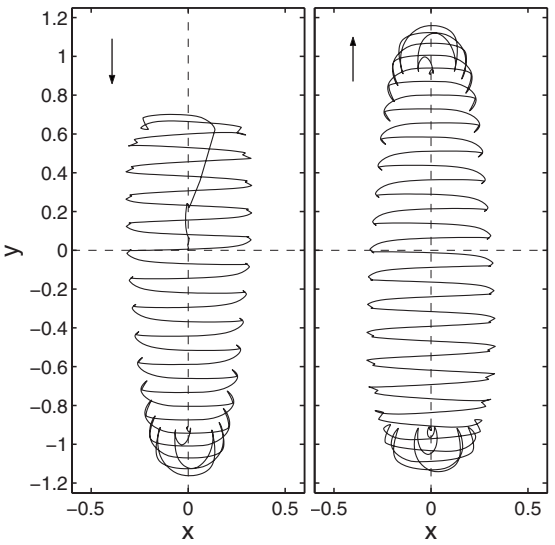

FIG. 10. Path of the vortex end when the tip oscillates along x with large amplitude and moves down from large positive $Y \geq 2$ to large-negative $Y \leq -2$ (left plot) and then moves up again to large positive $Y \geq 2$ (right plot). The straight vortex waits at $x=y=0$. When the tip approaches from above, the vortex end suddenly jumps to the tip and starts to oscillate with large amplitude, following the tip downwards. After some time the vortex end comes to a halt as in Figs. 5–7. When the oscillating tip approaches again from below, the vortex end starts to oscillate with slowly increasing amplitude along a path that looks similar to the path on which the vortex end came to a halt. The vortex paths shown at the lower left and at the upper right are nearly identical. The parameters are as in the left plot of Fig. 6.

is less than this pinning force, the vortex end remains pinned and does not move toward the tip. A more restrictive necessary condition for the vortex motion toward the tip is that the vortex can oscillate along x. This condition yields

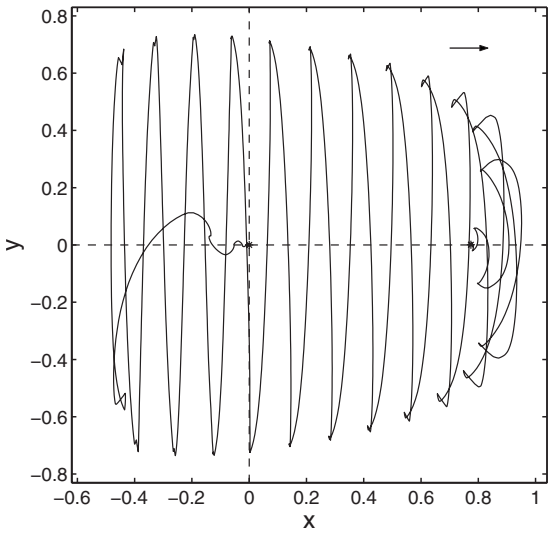

FIG. 11. Path of the vortex end for parameters as in the left plots of Figs. 6 and 10, but now the tip oscillates along y and approaches the vortex end (that waits at $x=y=0$) along x from far left ($X \leq -2$), moving further until the vortex end comes to a halt.

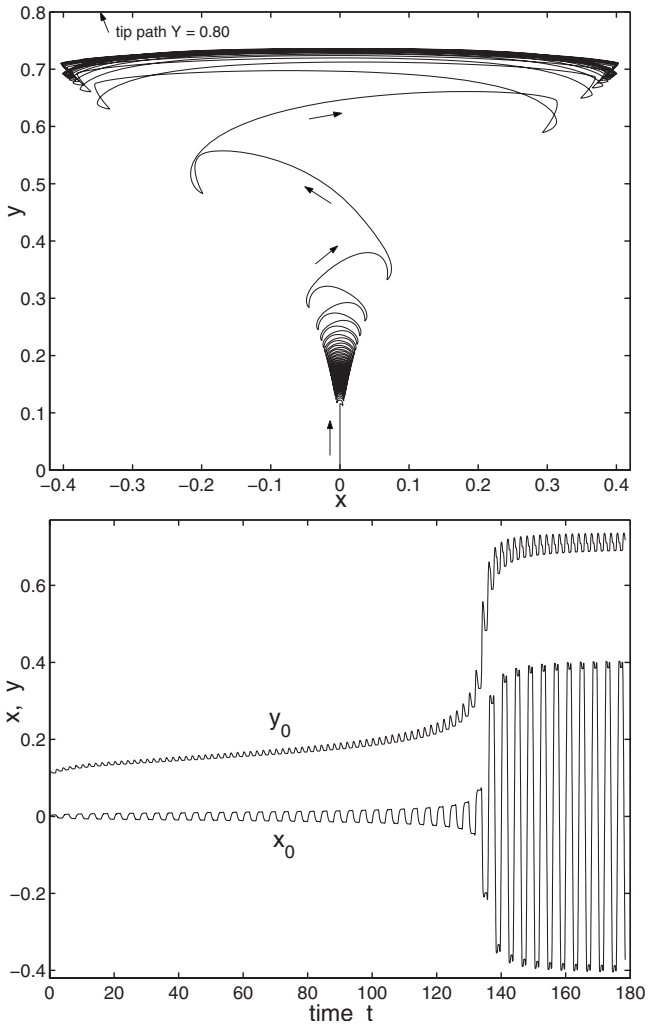

FIG. 12. Attraction of the vortex end to the oscillating tip. The magnetic tip oscillates with amplitude $a=1.4$ along the straight-line $Y=0.8$ parallel to the x axis, starting from $X=0$ at time $t=0$. When the tip approaches the starting point from large positive Y, the vortex end shifts to $y_0 \approx 0.11$, attracted by the tip. At $t>0$ the vortex end oscillates along x with small, slightly increasing amplitude, moving slowly to higher-y values. When $y_0 \approx 0.3$ is reached the vortex end jumps in a few big leaps to its maximum $y_0 \approx 0.73$. After that it oscillates on a stationary curve. The lower plot shows the temporal dependences of x_0 and y_0. All lengths in μm, the unit of t is a quarter of the tip period, the parameters are as in Fig. 10, but for simplicity we take $\zeta=1$ here.

$$[Y - y_0(0)]^2 \leq -\frac{(Z+h_0)^2}{2} + \sqrt{\frac{(Z+h_0)^4}{4} + \frac{q^2}{9F_p^2}}. \quad (28)$$

From numerical calculations we find (see Fig. 13) that there exists a distinct upper threshold for the distance $[Y-y_0(0)]$ between the vortex end and the tip-oscillation line at which the attraction process can occur, and this threshold is close to that given by Eq. (28).[14] If this threshold is indeed determined by the pinning forces and the dependence of the driving-force F on $X-x_0$ and $Y-y_0$ is known, this effect may allow sensitive measurements of these pinning forces acting on an individual vortex in type-II superconductors.

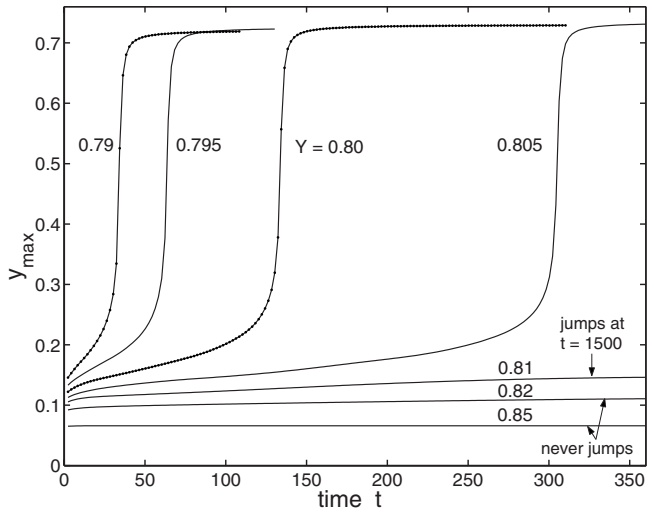

FIG. 13. Attraction of the vortex end (x_0, y_0) to the tip oscillating along x at constant Y as in Fig. 12 but for various distances $Y=0.79,\ldots,0.85$. Plotted is the maximum value $y_{\max}$ of y_0 in each half oscillation vs. time t. For $0.79 \leq Y \leq 0.81$ this $y_{\max}$ is slowly increasing and then suddenly jumps to a saturation value ≈ 0.73 within about five half oscillations. At $Y=0.81$ this steep jump occurs only at $t=1500$ (after 375 oscillations). For $Y \geq 0.815$, $y_{\max}$ saturates exponentially in t to a small value ≤ 0.114, and thus there is no jump. All parameters and units are the same as in Fig. 12.

When the tip oscillates, it generates currents whose orientation changes in time near the vortex, and the vortex motion toward the tip in Fig. 12 as well as the enhanced vortex response in the slow scan direction in Figs. 5–7 are reminiscent of the so-called longitudinal vortex shaking effect.[15] In this effect, in essence, a small ac current is superimposed perpendicularly to a dc critical current that flows in a sample. This leads not only to a periodic tilt of vortices but also to their *unidirectional* drift along the direction of the ac current and causes a dc electric field along the dc current. In the considered case of the oscillating tip the currents flow only near the surface of the superconductor, and only the upper, depinned part of the vortex "drifts."

IV. CONCLUSIONS

We derive equations that describe the deformation of an individual vortex in anisotropic type-II superconductors under the influence of the moving tip of a magnetic force microscope. These equations take into account the driving force generated by the tip, the elastic force caused by the vortex deformation, and the pinning force exerted by point defects. These equations are valid even at large deformations of the vortex, and they properly allow for the biaxial anisotropy of the superconductor. From these equations, we reproduce the main features of the experimental data obtained recently.[1] In particular, we explain the enhanced response of the vortex to pulling in the slow scan direction as compared to its response in the direction of the fast zigzag scan. We demonstrate that the vortex position at time t depends on the trajectory of the tip at previous times, and it is this property that eventually leads to the enhanced vortex response in the slow scan direction. We also point out that the enhanced anisotropy of pinning in the a-b plane that was observed in Ref. 1 is partly caused by the fact that the critical force at which the vortex starts to move depends on the angle θ of the vortex tilt and in general does not coincide with the pinning force.

We note a still unresolved problem. In order to obtain quantitative agreement of our calculations with the experimental data, we have to take a larger value of the vortex line tension than the value following from the theoretical estimate. The small line tension $\sim \varepsilon^2 \varepsilon_0$ of a vortex in an anisotropic bulk superconductor results from the almost complete cancellation of the increase in the length of a tilted vortex and the decrease of its energy per unit length, $e_l(\theta) \approx \varepsilon_0 \cos\theta$, with increasing tilt angle θ.[7] The existence of the surface at $z=0$ and of the tip changes the energy $e_l(\theta)$ in the surface layer of depth λ and, consequently, the almost complete cancellation does not occur there. The line tension of a vortex segment near the surface may thus be noticeably larger than the tension in the bulk. The discrepancy also may be due to the too simple expressions for the lateral driving force [see Eqs. (1) and (2)]. Since the penetration depth λ of the driving force should be on the order of λ_{ab}, this λ is comparable with the experimental values of $Z+h_0$. In this situation the correct driving force acting on a *curved* vortex at small distances $R \sim Z+h_0$ from the tip, is likely to be given by formulas more complicated than Eqs. (1) and (2). But Eq. (1) was, in fact, used in the experiment[1] for the extraction of the lateral driving force, which might lead to some overestimation of this force. Thus, a more detailed theoretical investigation of the driving force and the nonlocal line tension near the surface is needed.

One more problem that should be studied both theoretically and experimentally is the vortex-motion randomness that is superimposed on the regular vortex motion considered here. This randomness is clearly seen in the experimental data of Auslaender *et al.*[1] It is quite possible that apart from point defects and the weak collective pinning associated with them, in the sample there may be strong pinning centers, e.g., the clusters of point defects discussed in Ref. 1, that lead to the observed randomness.

ACKNOWLEDGMENTS

We thank Ophir Auslaender for discussions and for providing data. This work was supported by the German Israeli Research Grant Agreement (GIF) under Grant No. G-901-232.7/2005. E.Z. acknowledges the support of EU-FP7-ERC-AdG and of U.S.-Israel Binational Science Foundation (BSF).

APPENDIX A: FORMULAS FOR THE CRITICAL FORCE

Taking into account formulas (7) and (8), we obtain the following explicit form of Eqs. (11) and (12):

$$\tan\psi = \frac{N(\psi_1)}{D(\psi_1)}, \tag{A1}$$

$$f_c(\psi) = f_p(\psi_1)\left[1 + \frac{[\xi'(\theta,\varphi,\psi_1)]^2}{\xi^2(\theta,\varphi,\psi_1)}\right]^{1/2}, \tag{A2}$$

where $f_p(\psi_1)=f_p(\theta,\varphi,\psi_1)$ is given by Eq. (7), the prime means $d/d\psi_1$,

$$N = \eta \tan^3\psi_1 + 1.5\Delta\zeta \tan^2\psi_1 \cos\theta \sin 2\varphi + \tan\psi_1(2\eta_1 \cos^2\theta - \eta) - 0.5\Delta\zeta \cos\theta \sin 2\varphi,$$

$$D = \eta_1 \cos^2\theta + 1.5\Delta\zeta \tan\psi_1 \cos\theta \sin 2\varphi + \tan^2\psi_1(2\eta - \eta_1 \cos^2\theta) - 0.5\Delta\zeta \tan^3\psi_1 \cos\theta \sin 2\varphi,$$

$$\frac{|\xi'|}{\xi} = \frac{\Delta\zeta \cos\theta \sin 2\varphi \cos 2\psi_1 + \sin 2\psi_1(\eta - \cos^2\theta\eta_1)}{\Delta\zeta \cos\theta \sin 2\varphi \sin 2\psi_1 + 2\cos^2\psi_1 \cos^2\theta\eta_1 + 2\sin^2\psi_1\eta}, \tag{A3}$$

and $\Delta\zeta \equiv \zeta - \zeta^{-1}$, $\eta \equiv \eta(\varphi)$, and $\eta_1 \equiv \eta(\varphi+\pi/2)$. Equation (A1) permits one to find the auxiliary angle ψ_1 in terms of ψ, and then one can calculate f_c from Eq. (A2).

Let us define the parameter δ by the formula

$$2\delta \equiv \left(\frac{\eta}{\cos\theta} + \eta_1 \cos\theta - \sqrt{\left(\frac{\eta}{\cos\theta} + \eta_1 \cos\theta\right)^2 - 1}\right)^2. \tag{A4}$$

For example, if $\varphi=0$, one has $\delta=\cos^2\theta/\zeta^2$, while if $\varphi=\pi/2$, we obtain $\delta=\min[\cos^2\theta\zeta^2, (\cos^2\theta\zeta^2)^{-1}]$. If the parameter δ is larger than 1/2, there is a one-to-one correspondence between ψ and ψ_1. At $\delta<1/2$ the situation changes.[6] In this case spurious branches of $\psi_1(\psi)$ appear. The physical branch corresponds to a minimum value of f_c. For example, in the case $\delta\leq 1/2$ one finds the following expression for the critical force at $\psi=0$ and $\varphi=0$ or $\varphi=\pi/2$:

$$f_c(\psi=0;\varphi=0,\pi/2) = 2f_{p0}\sqrt{\delta(1-\delta)}, \tag{A5}$$

where $f_{p0}=f_p^c\sqrt{\zeta}$ at $\varphi=0$ and $f_{p0}=f_p^c/\sqrt{\zeta}$ at $\varphi=\pi/2$. On the other hand, at $\delta\geq 1/2$ one has $f_c(\psi=0;\varphi=0,\pi/2)=f_{p0}$ instead of formula (A5).

[1] O. M. Auslaender, L. Luan, E. W. J. Straver, J. E. Hoffman, N. C. Koshnick, E. Zeldov, D. A. Bonn, R. Liang, W. N. Hardy, and K. A. Moler, Nat. Phys. **5**, 35 (2009).

[2] U. H. Pi, Z. G. Khim, D. H. Kim, A. Schwarz, M. Liebmann, and R. Wiesendanger, Appl. Phys. Lett. **85**, 5307 (2004).

[3] A. M. Chang, H. D. Hallen, L. Harriott, H. F. Hess, H. L. Kao, J. Kwo, R. E. Miller, R. Wolfe, J. van der Ziel, and T. Y. Chang, Appl. Phys. Lett. **61**, 1974 (1992).

[4] G. Carneiro and E. H. Brandt, Phys. Rev. B **61**, 6370 (2000).

[5] Since the maximum F_{zm} of the force-component F_z occurs at $R=0$, Eq. (1) gives $F_m \approx 0.385F_{zm}$.

[6] G. P. Mikitik and E. H. Brandt, Phys. Rev. B **79**, 020506(R) (2009).

[7] E. H. Brandt, Phys. Rev. Lett. **69**, 1105 (1992).

[8] The use of formula (5) means that we neglect effects of the sample surface, $z=0$, and of the tip on the line tension of the vortex segment in the surface layer of thickness λ.

[9] T. Pereg-Barnea, P. J. Turner, R. Harris, G. K. Mullins, J. S. Bobowski, M. Raudsepp, R. Liang, D. A. Bonn, and W. N. Hardy, Phys. Rev. B **69**, 184513 (2004).

[10] At $z=0$ it is necessary to take into account the image of the vortex, and Eq. (16) means the absence of a sharp break in $x'(0)$ and $y'(0)$. Note that we allow for the effect of the sample surface on the vortex dynamics only in these boundary conditions.

[11] G. P. Mikitik and E. H. Brandt, Phys. Rev. B **71**, 012510 (2005).

[12] E. H. Brandt and G. P. Mikitik, Phys. Rev. B **76**, 064526 (2007).

[13] If the tip oscillates along y and slowly moves in the x direction, the shift of the vortex end in the slow scan direction x and the aspect ratio $\max(x_0)/\max(y_0)$ *decrease* with increasing anisotropy ζ.

[14] Equation (28) gives $Y-y_0(0)\leq 0.8$ for the parameters of Fig. 12, while the data of Fig. 13 reveal the threshold $Y-y_0(0)\approx 0.73$.

[15] G. P. Mikitik and E. H. Brandt, Phys. Rev. B **67**, 104511 (2003).